INDENV 2 (2025) 100073

Contents lists available at ScienceDirect

Indoor Environments

journal homepage: www.sciencedirect.com/journal/indoor-environments

Cyclone negative pressure pump for efficient purification of airborne contaminants

Gihyun Song [a], Kyungcheol Jang [a,b], Woobin Song [c], Wonchul Choi [d], Simon Song [c], Hyoungsoo Kim [a,*]

[a] Department of Mechanical Engineering, KAIST, Daejeon 34141, South Korea
[b] Department of Civil Urban Earth and Environmental Engineering, UNIST, UNIST-Gil 50, Ulsan 44919, South Korea
[c] Department of Mechanical Convergence Engineering, Hanyang University, Wangsimni-Ro 222, Seoul 04763, South Korea
[d] Korea Institute of Machinery and Materials (KIMM), Gajeongbuk-Ro 156, Daejeon 34103, South Korea

ARTICLE INFO

Keywords:
Air purification
Cyclone pump
Negative pressure
Airborne contaminants

ABSTRACT

Maintaining an isolation room with negative pressure is crucial in medical facilities to prevent the spread of airborne infections, especially during the COVID-19 pandemic. However, conventional negative pressure pumps have limitations in gathering suspended particles and controlling the airflow effectively. To resolve this issue, we developed a novel class of negative pressure pump that creates a swirling cyclone flow at the front to efficiently collect pollutants and particles, which was confirmed by a smoke visualization experiment. Based on the prototype pump, we conducted a numerical analysis to evaluate the particle collection performance of the cyclone pump in various scenarios, including patients covered with contaminants, and coughing or breathing. Our results demonstrate that the cyclone pump can purify airborne pollutants by up to 80%, offering superior performance over conventional pumps. We also identified optimal pump placement for effective particle purification. This research provides an innovative solution for improving the efficiency of negative pressure pumps and ventilation systems in medical settings, contributing to better control of airborne infections.

1. Introduction

The COVID-19 pandemic has had a profound impact on the world, with over 560 million people infected and more than 6 million deaths caused by severe respiratory symptoms [1]. While vaccination efforts have reduced the number of severe cases of the virus [2], the emergence of new variants continues to pose a threat to public health [3]. Airborne transmission of COVID-19 has been identified as a significant means of spreading the virus [4–9], particularly in hospitals where infected patients may require respiratory support that can aerosolize the virus [10].

It is well-known that COVID-19 viruses are transferred via respiratory droplets or aerosols [4–7]. Particularly, Jennison [5] showed that the patient acts as a massive atomizer of pathogens in 1942, and Papineni and Rosenthal [11] showed that breathing and coughing contain saliva droplets. Recently, Abkarian and Stone [12] further demonstrated that the saliva droplets and the pathogen aerosol could be generated by stretching and break-up of saliva filaments during a speech. They also showed that the speaking plosive sounds produce jetlike flows, causing the particles to travel more than two meters [13]. Bourouiba et al. [14] showed coughing or sneezing creates a turbulent cloud mixed with pathogen-laden particles that may travel several meters. These suspended viruses in aerosols or droplets could be viable and infectious for hours [8,15]. Therefore, to minimize the disease transfer, it is crucial to effectively get rid of the airborne contaminants in the air.

To prevent the spread of airborne contaminants in a confined area, a negative pressure (NP) condition is implemented. The NP rooms play a vital role in hospitals by controlling airflow and minimizing the transmission of pathogens between patient rooms and hallways [16,17]. These specialized environments rely on heating, ventilation, and air conditioning (HVAC) systems within the NP rooms. During periods of high infection rates, temporary or portable negative pressure pumps are deployed to meet the high demand for creating NP environment [18]. The purpose of NP rooms is to prevent pathogens from spreading to the anteroom [19]. Therefore, numerous studies have focused on HVAC ventilation methods to enhance the removal of indoor pathogens while maintaining the necessary negative pressure. In the previous research, it was shown that mixed ventilation approaches yield higher pathogen collection efficiency compared to displacement ventilation [20].

* Corresponding author.
E-mail address: hshk@kaist.ac.kr (H. Kim).

https://doi.org/10.1016/j.indenv.2025.100073
Received 5 August 2024; Received in revised form 5 November 2024; Accepted 2 January 2025
Available online 17 January 2025

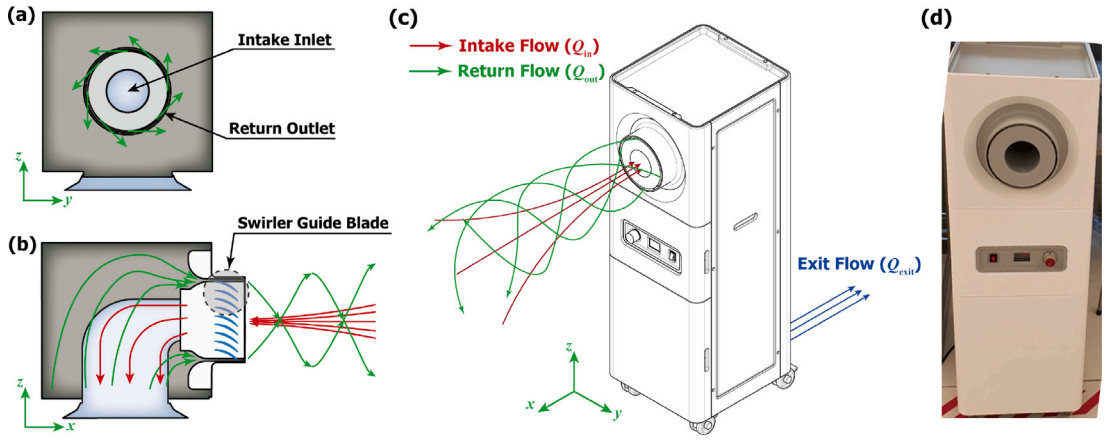

Fig. 1. Schematic diagram of the negative pressure pump of the cyclone. The cyclone negative pressure pump creates cyclone swirling flow with a combination of tangential return flow and nominal intake flow. (a) The front view of the cyclone negative pressure pump head. (b) The cross-sectional side view of the cyclone NP pump. The swirler guide blade creates a return flow that is tangential to an intake flow. (c) Illustration of the cyclone flows with the newly developed NP pump. The newly developed NP pump creates cyclone flows, with the red and green arrows representing the intake and swirl flow, respectively. The total exit flow rate, Q_{exit}, is purified by built-in HEPA filters and then expelled through the bottom back outlet port. (d) Cyclone swirler type negative pressure pump. (For interpretation of the references to color in this figure legend, the reader is referred to the web version of this article.)

To enhance the effectiveness of mixed ventilation systems, researchers have delved into various strategies, including strategically positioning NP pump inlets and ventilation outlets [21], as well as determining optimal air circulation rates per hour (ACH) [22–24]. Nonetheless, traditional NP pumps, whether integrated into HVAC systems or utilized in portable setups, have limitations in efficiently filtering airborne pathogens due to their low suction rate. The main drawback arises from the use of front-located filter-oriented structures, which cause significant pressure drops due to HEPA filters [25,26]. Furthermore, the slow flow speed of these pumps hinders effective collection and purification of airborne contaminants disrupted by medical staff movements. This could potentially lead to airborne pathogen-laden particles lingering for extended periods [27].

To address the aforementioned challenges, this study introduces a newly developed negative pressure pump that utilizes a cyclone flow at the inlet, resulting in a more effective collection of pollutants. Inspired by the characteristics of natural cyclones, which possess a low-pressure center and powerful tangential winds driven by the Coriolis force [28], our design incorporates a similar swirling turbulent and directional flow to enhance pollutant collection efficiency.

In Section 2, we provide a comprehensive description of the cyclone flow creation process. In Sections 3 and 4, we provide numerical analysis and methodology to compute the cyclone flow of our NP pump. To validate our numerical simulations, we analyzed the cyclone flow of the pump using smoke particle image velocimetry (PIV) in Section 5. Furthermore, to compare the performance of our cyclone pump with that of a conventional pump, we conducted numerical simulations for three scenarios in Section 6: a patient covered in pathogen-laden particles, a patient breathing, and a patient coughing.

The results of our study demonstrate that the cyclone NP pump effectively collects airborne particles, even in situations where medical staff moves around the patient. This innovative solution provides a safer and more efficient approach to controlling airborne pathogens in negative pressure rooms.

2. Cyclone negative pressure pump

The cyclone NP pump incorporates a swirler design to create a swirling flow based on the principles of a natural cyclone, depicted in Fig. 1. The pump features a fan that generates the main suction (Q_{in}) via a circular intake inlet. The incoming air is then filtered by HEPA filters, and some portion of the incoming air flow is redirected to the swirler guide blades to create a tangential return flow (Q_{out}) through the return outlet at the pump head. The interplay between the suction and return flows creates a swirling flow at the inlet, which efficiently captures indoor air pollutants. The total exit flow rate of air ($Q_{exit} = |Q_{in} - Q_{out}|$) which is difference between Q_{in} and Q_{out}, is purified by the built-in HEPA filters of the cyclone NP pump. Then the total exit flow rate of air (Q_{exit}) eventually expelled outside through the outlet port of the cyclone pump. Detailed sketches of the cyclone NP pump can be found in Fig. 1(a) and 1(b), while Fig. 1(c) provides an illustration of the cyclone swirling flow generated by the NP pump, which was utilized in medical facilities during the COVID-19 pandemic in South Korea. The actual cyclone NP pump is illustrated in Fig. 1(d) and the pump's test operation is shown in Fig. 2 and Supplementary Movie 1. This machine is able to create −15 Pa environment in 33 m^3 volume room under maximum conditions. The pump can maintain a −5 Pa environment with a noise level of about 55 dB. In terms of power consumption, the pump uses 135 W at maximum fan mode and 20 W in steady fan mode. This device is patented in South Korea [29].

To generate a cyclone flow, it is crucial to have the optimal flow rate ratio between the intake flow (Q_{in}) and the return flow (Q_{out}). To determine the optimal flow rate ratio for the NP pump, we conducted a flow visualization experiment using a smoke generator (SFM-3000, Hongkong Gesida Electronic Technology) and a 10 W continuous laser source (MGL-V-532-10 W, Changchun New Co.), as shown in Fig. 2(a) and 2(b). We varied the flow rate ratio from 1 to 5 [See Supplementary Figure. S1] and confirmed that the NP pump can generate the proper cyclone flow at a ratio of 3 [See Fig. 2(c) and 2(d)] for smoke flow visualization results, which was experimentally determined.

3. Numerical analysis

We conducted a numerical analysis of the air purification performance of the current cyclone NP pump to explore the impact of the current pump on the purification of indoor contaminants. To simulate the situation of a patient transfer scenario to a hospital, we considered a situation that a respiratory disease patient laid on a bed with medical staff in a confined NP room. Here, the computational fluid dynamics (CFD) domain for the cyclone negative pressure pump is shown in Fig. 3(a) and 3(b), where the considered room volume was 4 m × 4 m × 2.5 m. For simplicity and computational cost, cuboid models of the patient and medical staff were used (see Table 1).

To define the flow and boundary conditions for the NP pump, we used the information and specifications of the conventional NP pump of the Korea Cancer Center Hospital. The pump head and the inlet were

Table 1
Physical dimensions of CFD domain.

Name	*x*-directionlength (m)	*y*-directionwidth (m)	*z*-directionheight (m)
Room	4.0	4.0	2.5
Bed	2.0	0.9	0.2
Bed-leg	0.1	0.1	0.85
Walking Healthcare Taker			
Body	0.2	0.3	0.675
Head	0.2	0.15	0.305
Arms	0.2	0.1	0.575
Legs	0.2	0.1	0.75
Patient on a bed			
Mouth	0.04	0.04	–
Body	1.73	0.5	0.2
Conventional NP pump head			
Intake inlet	–	1.2	1.2
Cyclone NP pump head	Inner diameter (mm)	Outer diameter (mm)	
Intake inlet	–	40	
Return outlet	75	80	

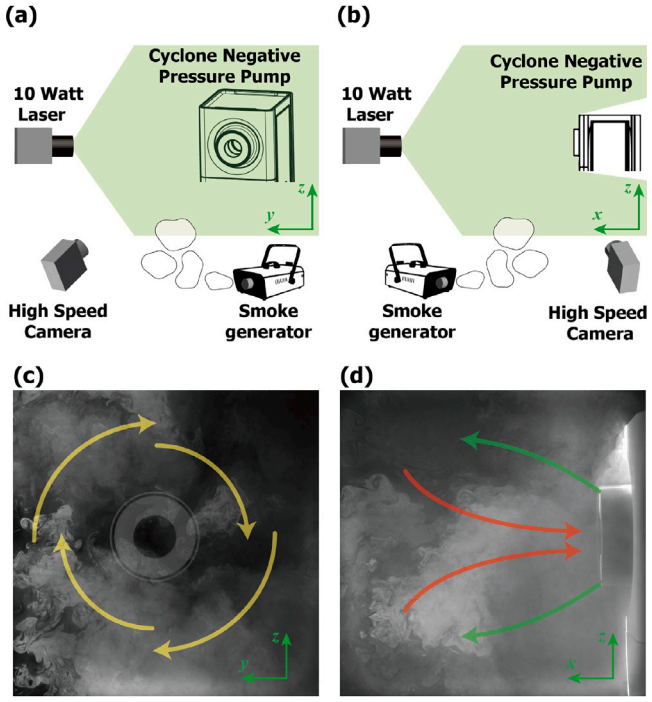

Fig. 2. Flow visualization experiment to determine the optimal flow rate ratio for the cyclone NP pump. Schematic of the flow visualization experiment using a smoke generator and a 10 W continuous laser source showing (a) front view and (b) side view of the cyclone NP pump. Experiment results showing (c) front view and (d) side view of the visualization results. Yellow arrows indicate the typical cyclone flow pattern generated by the NP pump, while red arrows indicate the suctioning intake flow and green arrows indicate the tangential return flow, which is essential for creating the cyclone flow. (For interpretation of the references to color in this figure legend, the reader is referred to the web version of this article.)

located 1.4 m above the floor of the room in Fig. 3(c). The ventilation inlet supplied fresh air at a rate of 9 ACH (air changes per hour) using a mass-flow-inlet boundary condition. To satisfy the negative pressure of −5 Pa [30], the pressure-outlet boundary condition was set for the intake inlet(see Table 2)

To compare our results with literature studies [31,32], we considered that the medical staff walked along the patient where we defined the staff as a walking healthcare taker (WHT), as sketched in Fig. 3. The WHT was placed on the right side of the patient and walked toward the wall of the ventilation inlet with a walking speed of 0.5 m/s for 4.6 secs [33]. To investigate additional possible situations in a hospital, we will consider the breathing and coughing of the patient (see the section of Results and Discussion). To simulate this, we assumed that the patient had a mouth size of 4 cm × 4 cm facing vertically to the ceiling of the room. The velocity of the patient's breathing and coughing was modeled using a user-defined function (UDF) and the direction was normal to the surface of the mouth.

Table 2
Boundary conditions for CFD domain.

Boundaries	Boundary types	Cases	Value	Unit
Ventilation inlet	mass-flow-inlet	Cyclone NP Conventional NP	4.0834 6.1561	kg/min
Return outlet	mass-flow-inlet	Cyclone NP	2.0417	kg/min
Patient body	wall (heat-flux)	Both	46.5	W/m^2
Intake inlet	pressure-outlet	Both	−5	Pa
Mouth	velocity-inlet	Both	UDF	m/s

The cyclone NP pump had both concentric intake inlet and return outlet [See Fig. 1(a)], with radii values listed in Table 1, to create a cyclone flow. To satisfy the flow rate ratio of 3 between intake inlet and return outlet (validated from the experiments), the return outlet had a flow rate of 2.0417 kg/min for the cyclone NP case. The mass-flow-inlet boundary type was set for the return outlet with a tangential 30-degree to axial flow direction applied. On the other hand, the conventional NP pump had the same flow rate for both intake and ventilation inlets since it had no return outlet. For your information, the conventional NP pump merely drew in the indoor airflow at a very low speed.

Here, we considered that while the thermal plume of the patient was set at 46.52 W/m^2 [31,32], the WHT body's thermal buoyancy effect was neglected because forced convection by the wake of the WHT is dominant at a walking speed over 0.2 m/s [34] (see Table 2).

4. Numerical methodology

In this study, the commercial CFD software ANSYS Fluent v17.2 was utilized to simulate the negative pressure room and the pump. For the turbulence model, direct numerical simulation (DNS) or large eddy simulations (LES) requires considerable time and cost [35]. A realizable $k-\epsilon$ Reynolds-Averaged Navier–Stokes (RANS) turbulence model, which is widely used for indoor turbulence flow due to its economical advantages and robustness, was adopted for indoor airflow simulations [31,36,37].

The general format of the governing equations for continuity, momentum, energy, turbulent kinematic energy k, and turbulent dissipation energy ϵ is as follows:

$$\frac{\partial}{\partial t}(\rho k)+\frac{\partial}{\partial x_j}(\rho k u_j)=\frac{\partial}{\partial x_j}\left[\left(\mu+\frac{\mu_t}{\sigma_k}\right)\frac{\partial k}{\partial x_j}\right] + G_k+G_b-\rho\epsilon-Y_M+S_k, \quad (1)$$

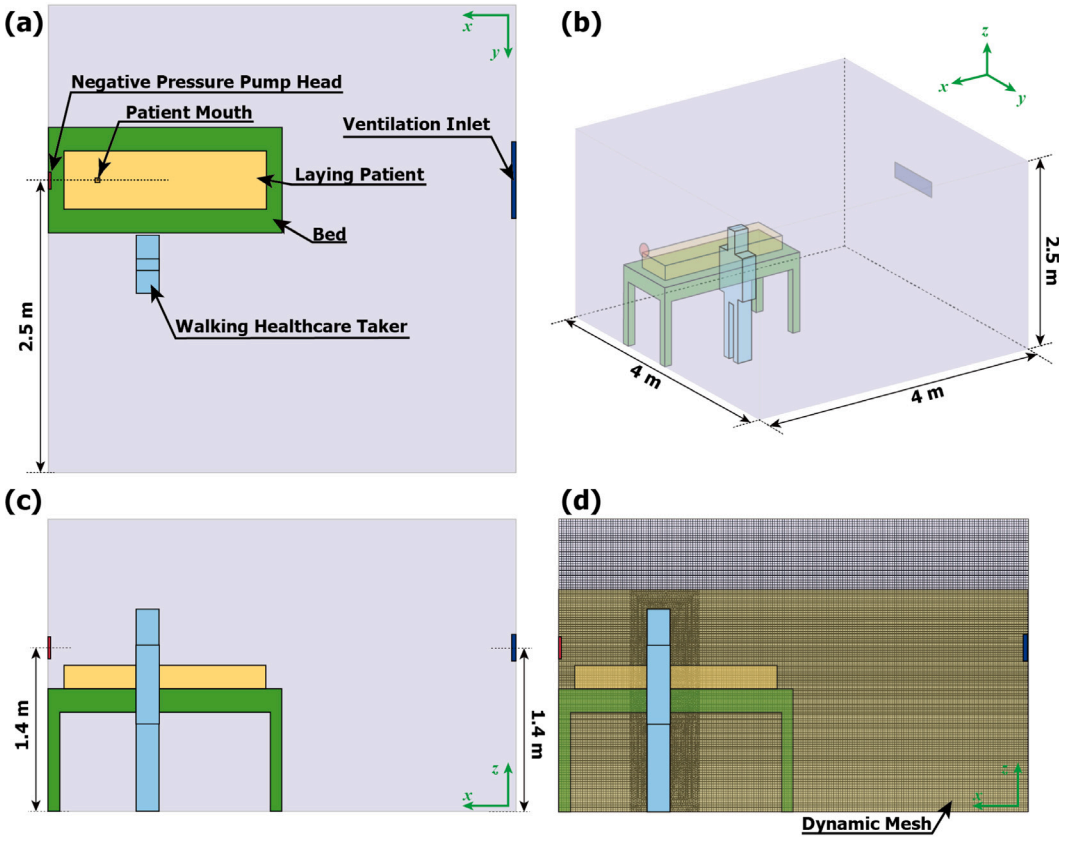

Fig. 3. CFD domain for the negative pressure room with the NP pump. (a) Top-view and (b) 3D isometric view. (c) The side-view and (d) mesh domain of (c). The head of the NP pump is located on the wall of the domain, and the walking healthcare taker (WHT) moves toward the ventilation inlet wall with a walking speed of 0.5 m/s. Here, the CFD domain having 5.5 million mesh cells is determined from the grid dependence test.

$$\frac{\partial}{\partial t}(\rho\epsilon)+\frac{\partial}{\partial x_j}(\rho\epsilon u_j)=\frac{\partial}{\partial x_j}\left[\left(\mu+\frac{\mu_t}{\sigma_\epsilon}\right)\frac{\partial\epsilon}{\partial x_j}\right] + \rho C_1 S_\epsilon-\rho C_2\frac{\epsilon^2}{k+\sqrt{\nu\epsilon}} + C_{1\epsilon}\frac{\epsilon}{k}C_{3\epsilon}G_b+S_\epsilon, \tag{2}$$

where $\mu_t=\rho C_\mu k^2/\epsilon$, $C_1=\max\left[0.43,\eta/(\eta+5)\right]$, $\eta=Sk/\epsilon$, and $S=\sqrt{2S_{ij}S_{ij}}$. Here, ρ is the density of the air, μ is the viscosity of the air, μ_t is the turbulent viscosity by combining k and ϵ. u_j is a velocity vector that represents in the x, y, and z directions. For the $k-\epsilon$ turbulent model, G_k and G_b represent the generation of turbulence kinematic due to the mean velocity gradients and the generation of turbulence kinematic energy due to buoyancy, respectively. Y_M is the contribution of the fluctuating dilatation in compressible turbulence to the overall dissipation rate. σ_k and σ_ϵ are the turbulent Prandtl numbers for k and ϵ, respectively. S_k and S_ϵ are the user-defined source terms.

For the pressure–velocity coupling equations, the semi-implicit method for the pressure-linked equations (SIMPLE) algorithm was utilized. The Boussinesq equation was used to calculate the air density considering the buoyancy effect of a thermal plume of the patient.

Saliva ejecta has a wide range of its size, though droplet size larger than 100 μm settles fast due to the gravitational effect. Khosronejad et al. [38] showed that the ejected saliva particles ranging $O(0.1\sim10)$ μm, which are large enough to carry the virus, undergo fast evaporation while those are in the air. They showed that the ejected particles shrink, and keep their size of 0.1 μm after 0.2-s evaporation [38]. Since the evaporation time is much shorter than our CFD time regime, we neglected the saliva evaporation and considered the saliva particles to be kept at 0.1 μm as tracer particles.

To simulate the motion of saliva droplets, a discrete phase model (DPM) was used. The DPM model tracks particles separately through the flow domain by solving the force balance equation of particle movement. Based on the literatures [39,40], the following assumptions and simplifications were adopted in this study: (a) the evaporation of droplets was not considered due to fast evaporation time; (b) heat and mass transfer between air and droplet was negligible; (c) droplets were captured on solid surfaces; (d) coagulation effect of droplets was neglected [39]; and (e) all droplets were spherical solid particles. The force balance between air and the particle in the j-direction (x, y, and z-directions) is expressed as follows [40],

$$\frac{\mathrm{d}u_{pj}}{\mathrm{d}t}=\frac{18\mu}{\rho_p \mathrm{d}_p^2}\frac{C_D\mathrm{Re}}{24}(u_j-u_{pj})+\frac{g_z(\rho_p-\rho)}{\rho_p}+F_{aj} \tag{3}$$

where u_{pj} is the particle velocity in the x, y, and z directions, d_p is the particle diameter, g_z is the gravitational term, ρ_p is the particle density, and the F_{aj} is the additional acceleration term acting on the particle. Here, Re is the relative Reynolds number, $\mathrm{Re}=\rho \mathrm{d}_p|u_{pj}-u_j|/\mu$. In this study, the additional acceleration terms included pressure gradient force, Brownian force, and Saffman's lift force [37]. Those forces are relatively large for indoor airflow compared to other forces: Basset force and virtual mass force [41]. The pressure gradient force can be written as $F_{aj}=\frac{1}{2}\frac{\rho}{\rho_p}\frac{\mathrm{d}}{\mathrm{d}t}\left(u_j-u_{pj}\right)$. The amplitudes of the Brownian force components are modeled as a Gaussian white noise process, $F_{bj}=\zeta_j\sqrt{\pi S_0/\Delta t}$, where $S_0=(216\nu k_B T)/[\pi^2\rho \mathrm{d}_p{}^2(\rho_p/\rho)^2 C_c]$ where ζ_j are non-mean, unit-variance-independent Gaussian random numbers. Here, ν is the kinematic viscosity of the fluid, T is the absolute temperature of the fluid, k_B is the Boltzmann constant, and C_c is the Cunningham correction coefficient to Stokes' drag law. The Saffman's lift force is $F_{sj}=\left(2K\nu^{1/2}\rho d_{ij}\right)\left(u_j-u_{pj}\right)/\left[\rho_p \mathrm{d}_p\left(d_{lk}d_{kl}\right)^{1/4}\right]$ where $K=2.594$ and d_{ij} is the deformation tensor.

The dynamic mesh model was utilized to simulate the airflow affected by the WHT, and the integral form of the conservation equations

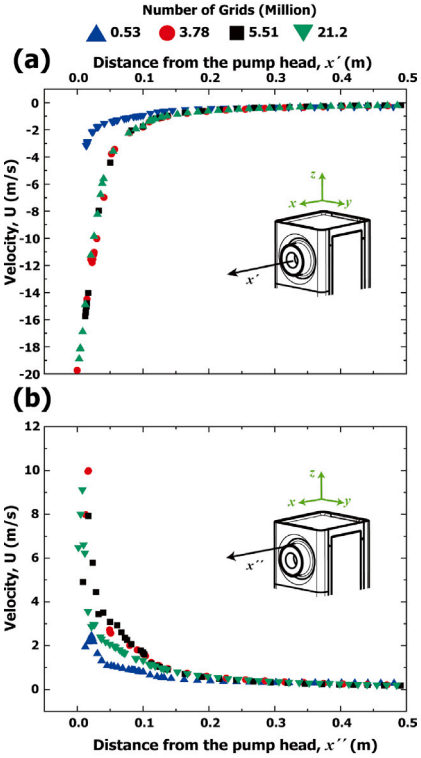

Fig. 4. Grid test results from four different mesh conditions. The velocity was achieved from (a) the center line along the black arrow at the center of the inlet and (b) the top line of the head of the cyclone negative pressure pump along the black arrow. The intake flow is considered negative as the cyclone pump suctions indoor air, while the return flow is positive, representing the incoming flow that generates the swirling effect. Each of the lines is illustrated in the inset of each graph. Here, the black arrows are normal to the yz-plane of the cyclone NP pump.

Table 3
Grid independence test.

Number of grid (million)	Max. skewness	Continuity residuals	Other residuals
0.53	0.93	$> 10^{-2}$	$> 10^{-3}$
3.78	0.81	$> 10^{-3}$	$> 10^{-5}$
5.51	0.76	$< 10^{-3}$	$< 10^{-6}$
21.2	0.7	$< 10^{-3}$	$< 10^{-6}$

of dynamic meshes is expressed as follows [37],

$$\frac{\mathrm{d}}{\mathrm{d}t}\int_V \rho\phi \mathrm{d}V + \int_{\partial V} \rho\phi(\vec{u}-\vec{u_g})\cdot \mathrm{d}\vec{A} = \int_{\partial V} \rho\Gamma\nabla\phi\cdot \mathrm{d}\vec{A} + \int_V S_\phi \mathrm{d}V \tag{4}$$

where $\vec{u}$ is a velocity vector, ϕ is the general scalar. Γ represents the effective diffusion coefficient, and S_ϕ is the source term for each dependent variable. $\vec{u}_g$ is the grid velocity of the moving mesh and ∂V is the boundary of arbitrary control volume V [37].

The entire CFD domain was created using hexahedral meshes, with a wedge-shaped mesh used near the WHT, as shown in Fig. 3(d). To maintain a constant grid size in the dynamic mesh zone, the dynamic layering method was employed. This method allowed the resolution of the computation cell adjacent to a moving boundary to adjust based on the height of the layer next to the moving surface [37]. The dynamic meshes were limited to the yellowish zone in Fig. 3(d), while the other meshes remained static. We conducted a grid independence test, as shown in Table 3. To check the grid test results, we compared the velocity magnitude profiles along the center line of the inlet and the top line of the outlet of the cyclone NP pump (see the results in Fig. 4). Based on the grid test, we confirmed that a 5.5 million grid system would be satisfied for the numerical computation.

For the unsteady calculation, we used a time step of 0.001 s, which satisfied the Courant–Friedrichs–Lewy number below 1. We implemented a walking model of WHT and a breathing and coughing model of the patient using a UDF (user-defined function).

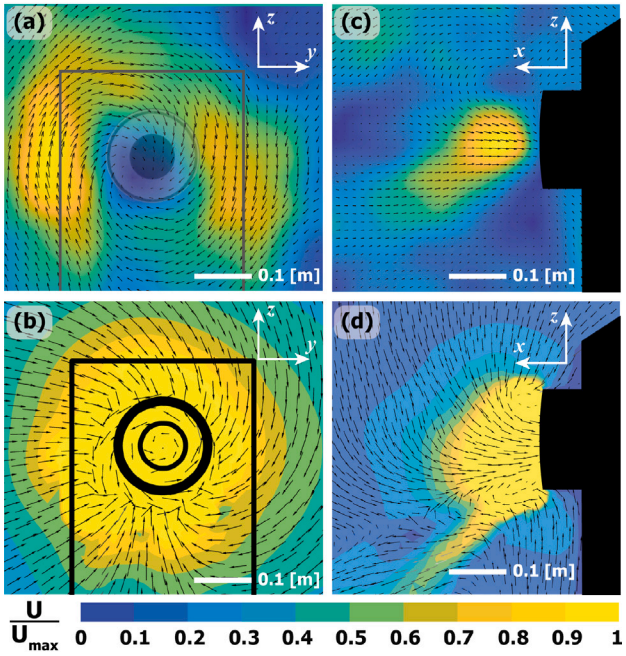

Fig. 5. Comparison of front and side flow patterns between (a), (c) experimental (PIV) and (b), (d) numerical results of the cyclone NP pump. For the front flow patterns shown in (a) and (c), data were taken from a plane offset by 0.15 m from the pump head. The side flow patterns in (b) and (d) were obtained from the center plane of the cyclone pump head. Details of the smoke flow visualization experiment are provided in Fig. 2. Black arrows in both sets of results represent flow patterns, with velocity magnitude (U) normalized to the maximum velocity (U_{max}) for each case.

5. Flow visualization using smoke PIV

To further verify the CFD results, we performed time-resolved smoke flow visualization techniques based on the particle image velocimetry (PIV) method. The experimental and numerical results are presented in Fig. 5. For the flow field measurement, smoke was used as tracer particles. The size of the smoke particles ranges from $O(1 \sim 10)$ μm, with a density of $O(1)$ g/mL. The Stokes number, representing the ratio between the characteristic time of a particle and that of the flow, is much smaller than unity for smoke particles. Therefore, PIV using smoke particles provides an accurate representation of the flow field measurements. The smoke tracer was excited at a wavelength of 532 nm by the Nd: YAG laser. The excited smoke signal was captured using a high-speed camera (Fastcam, Mini-AX200, Photron, Japan). Sequential images of the excited smoke tracers were recorded using the camera that captured 500 frames per second. Since the major cyclone flow generated by the NP pump occurred in front of the pump head, coexisting with the inlet and outlet, the focal plane was set at 15 cm offset from the surface of the pump head. The PIVlab tool [42] in MATLAB was used for flow field calculations. To obtain vector fields, we applied iterative 2D cross-correlation of the tracer images with multiple interrogation windows of 128 × 128 pixels (first) and 32 × 32 pixels (second) with 50% overlaps, where the signal-to-noise ratio (SNR > 3) was satisfied for reliable PIV [43].

We compared the front flow patterns from the smoke PIV experiments (a, c) and numerical simulations (b, d), as shown in Fig. 5. Fig. 5(a) and 5(c) display the front flow patterns of the cyclone NP

pump, while Fig. 5(b) and 5(d) show the side flow patterns. The velocity magnitude U was normalized by the maximum velocity U_{max} to validate the cyclone flow pattern. From Fig. 5(a) and 5(c), both results confirmed the azimuthal gyration flow pattern, indicating that the numerical methodology effectively simulated the cyclone flow. Additionally, the side flow patterns in Fig. 5(b) and 5(d) confirmed the strong suction intake flow.

However, in the front flow patterns, the flow center did not align well due to limitations of the two-dimensional PIV experiment, which cannot capture out-of-plane velocity components. The intense suction flow of the cyclone NP pump, as shown in Fig. 5(b) and 5(d), caused the smoke tracer to dissipate quickly as it was rapidly drawn into the intake inlet. This rapid dissipation prevented the tracer from being sustained over extended periods, resulting in a lack of intake velocity information at the center in the PIV results.

Additionally, the numerical simulation was performed under ideal steady-state conditions, whereas the actual cyclone NP pump was not in a perfect steady state due to the rotating turbo fans inside the pump. As a result, the return flow rate at the outlet was not entirely uniform along the azimuthal direction (see Fig. 1 and Supplementary Movie 1). Despite these limitations, the cyclone flow was well reproduced using the numerical boundary conditions, leading us to believe that CFD can effectively simulate particle collection performance in different scenarios.

6. Results and discussion

Building upon the validation of our numerical simulations through PIV analysis in Sections 4 and 5, we now direct our attention to a comprehensive evaluation of the particle collection performance of the cyclone NP pump in this section. To examine the pump performance, we considered three possible situations in a hospital.

World Health Organization (WHO) recommended that COVID-19 patients should be transported to designated health facilities by ambulance or repurposed vehicles [44]. During the patient transfer, the driver's cabin and patient compartment are sealed and separated. Patients continuously generate saliva droplets through breathing and coughing [11], which may contaminate their body surface [8]. Following the transfer, patients are placed in negatively pressurized isolation care units, where they continue to produce saliva droplets through breathing and coughing. It is noteworthy that approximately 70% of COVID-19 patients experience coughing [45].

In the subsequent sections, we conducted a detailed evaluation of the cyclone NP pump's performance in three distinct scenarios that occur after patient transport to healthcare facilities: Case (1) patient's body covered by pathogens, Case (2) patient producing pathogens through breathing, and Case (3) patient producing pathogens through coughing. We compared the collection efficiency of the NP pump to the conventional case by investigating these three scenarios using particle collection efficiency. To quantitatively compare two pumps, we investigated the particle collection efficiency using the following equation,

$$\left[\begin{matrix}\text{Collection}\\ \text{Efficiency}\end{matrix}\right] = \frac{\text{No. of collected particles}}{\text{No. of total particles}} \times 100\,[\%]. \tag{5}$$

This metric forms the basis of our investigation, where higher collection efficiency indicates a more effective rate of particle collection. Our motivation for this evaluation stems from the belief that a high particle collection rate can significantly lower the risk of infection transmission. Respiratory diseases are transmitted through airborne pathogen particles that contain viral loads [46]. Infection occurs when a sufficient amount of viral load enters a potential host [47,48]. Therefore, reducing airborne particle concentration is crucial in minimizing the likelihood of infection [49,50].

6.1. Case 1: A patient contaminated with pathogens

For the first scenario, we considered the situation that a respiratory disease patient was just hospitalized in a negatively pressurized room. In this case, we assumed that the patient's body was contaminated with pathogen-laden particles during the medical transfer, represented as red-colored dots on the patient's body surface as presented in Fig. 6(a). We simulated how these particles were agitated in the room while the WHT moved next to the patient at 0.5 m/s, which was the same situation of the literature cases [32,33]. From the numerical simulation, we observed that the vortical flow structure behind the WHT by walking mixed and spread the airborne particles in the room, as shown in Fig. 6(b), which was consistent with the literatures [31,32]. The agitating motion caused the contaminated particles to spread throughout the NP room. While the conventional NP pump slowly drew in the particles, the cyclone NP pump rapidly collected them, as indicated in Fig. 6(c). In both cases, the airborne particles spread due to external effects, *i.e.*, the movement of the WHT and the pump.

Nevertheless, during the first 25 secs, the two pumps showed a dramatic difference. While the conventional pump can only clean 10% of pollutants, the cyclone pump can purify 50% [see Fig. 6(c)]. The conventional pump cannot rapidly collect airborne particles due to the low flow speed. This means that less airborne particles remained in the case of the cyclone pump, so that the particles concentration is far less than the conventional one. From the previous studies, lowering pollutants concentration is a critical factor not to infect respiratory disease since infection requires a certain amount of viral dose entering possible patients [48,50]. Therefore, the rapid clean by the cyclone pump can lower the secondary transmission.

Although the two cases showed a similar collection efficiency of around $t = 200$ s, the indoor air should be completely different. Because, for the cyclone NP pump case, airborne particles were diluted and dispersed entirely in the room. For the conventional pump case, the highly concentrated particles were under the patient's bed and in the corner of the room, as shown in Fig. 6(a). If WHT walks through this highly concentrated area, then the motion of WHT will redisperse and agitate those particles sequentially. This situation can increase the possibility of secondary transmission since airborne pathogens would be viable and infectious for hours [8,15]. So, in this situation, the cyclone NP pump might provide an immediate and effective ventilation impact [46,47,49].

6.2. Case 2: Producing pathogen particles through breathing by an infected patient

Next, we examined a scenario in which a patient with a respiratory disease constantly exhaled droplets of saliva while breathing [11]. Based on the literature [38], we assumed that the patient emitted particles with a breathing cycle with a maximum speed, V_{max}, of 0.89 m/s through the patient's mouth of 4 cm × 4 cm. The flow speed of the breathing cycle was assumed to have a sinusoidal function with breathing frequency f (=1/5 sec^{-1}),

$$V(t) = V_{max}\sin(2\pi f t) \tag{6}$$

In this simulation, the patient kept emitting the particles by breathing as shown in Fig. 7(a). Here, we only considered one period of breathing for the numerical study. For the conventional NP pump, particles expelled by breathing were dispersed towards the ceiling of the room without any particle collection by the pump in $t = 5$ s, as shown in Fig. 7(a). The suction flow rate by the conventional pump was not enough to capture the particles. Expelled pathogen particles diffused into the room without disturbance. While the conventional NP pump demonstrated poor cleaning performance, the cyclone NP pump effectively collected almost all particles where the suction rate of the cyclone swirling flow was predominant compared to the breathing flow, as shown in Fig. 7. The cyclone NP pump showed 85% air purification within 5 secs. The efficient particle collection helps to create a safe environment for WHT.

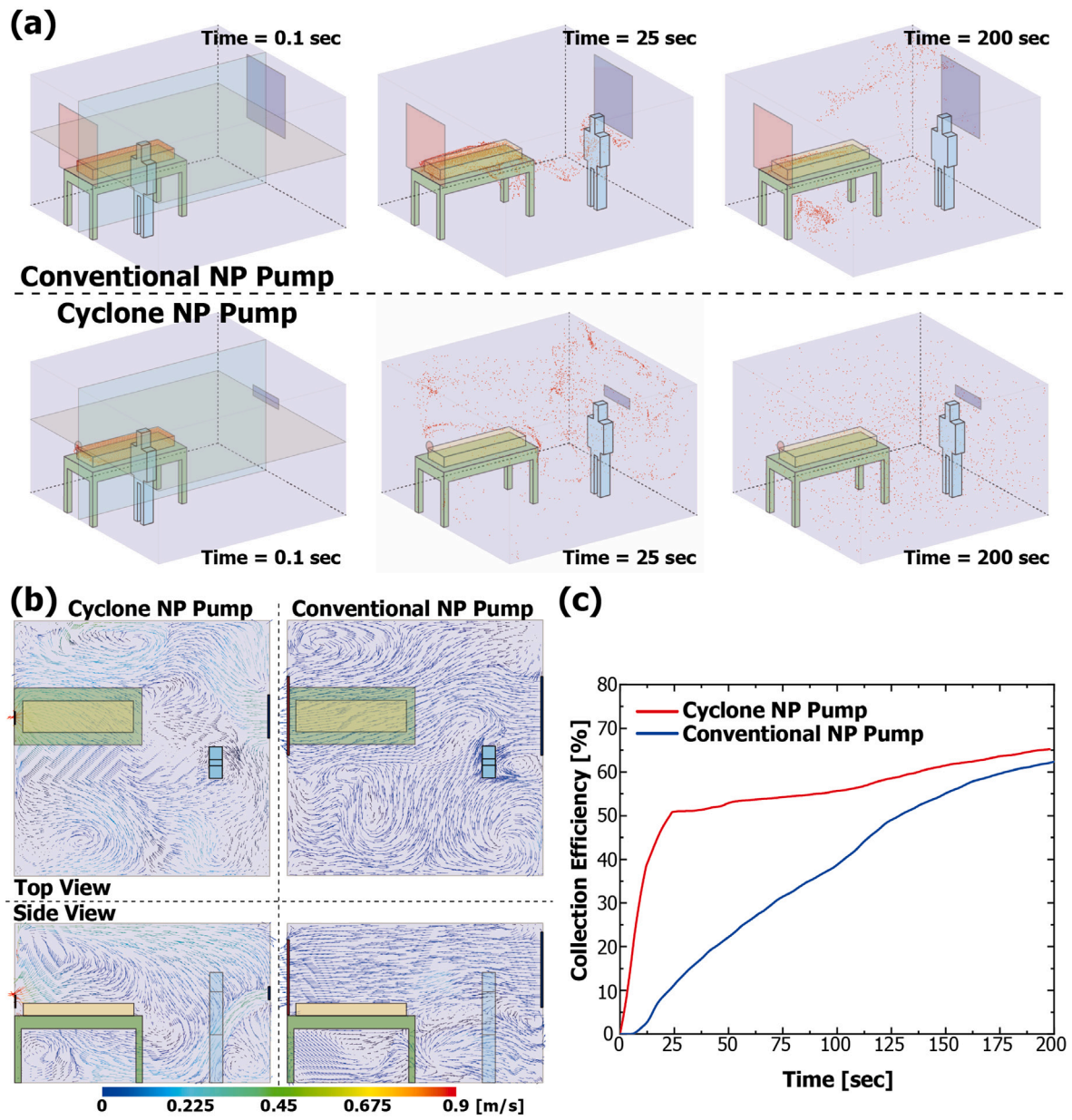

Fig. 6. First scenario: Pathogen-contaminated patient. The particle-collecting performance between the conventional NP pump and the cyclone NP pump was investigated. (a) Distribution of pollutant particles at t = 0.1, 25, and 200 s (b) Comparison of the velocity vector fields at the vertical plane and the horizontal plane. The cross-sectional planes are depicted in (a). (c) Particle collection efficiency for the cyclone NP pump and conventional NP pump. See Supplementary Movie 2.

6.3. Case 3: Producing pathogen particles through coughing by an infected patient

Lastly, a significant symptom of the respiratory disease patient could be a cough [45]. Based on the literature, when people cough, the expelled human saliva droplets have a wide range of ejecta speed, such as O(1–10) m/s [51]. It is known that coughing and sneezing emit turbulent multiphase flow and create a complicated fragmentation process of saliva droplets, which can produce countless airborne droplets [52]. To numerically evaluate the particle collection efficiency in this case, we chose the coughing conditions based on the literature conditions. We mainly considered the coughing speed ($V_{\max}$) and its frequency ($f = 2\,\mathrm{s}^{-1}$), *e.g.*, $V(t) = V_{\max}\sin(2\pi f t)$. The airborne droplet size was assumed to be around 0.1 μm [38]. Based on the literature [53], it is reported patients can expel pathogen-laden particles within just 0.5 s when coughing with maximum coughing speeds reaching about 10 m/s [54,55]. Simulating this frequent and rapid coughing features is very challenging because it requires periodic jet-like turbulent flow [13] and droplet atomization process [12], both of which are extremely difficult to model in numerical simulations, especially when considering indoor airflow. Therefore, in this study, we primarily focused on the collection of dispersed particles in a negative pressure room, depending on the type of negative pressure pump used.

In the case of coughing, we realized that a single-cyclone NP pump placed on the head side was insufficient to collect the pathogen particles effectively. As shown in Fig. 8(a), the single-cyclone NP pump near the head of the patient could not help to collect the cough particles. This was because the coughing speed was much faster than the suction flow speed of the single-cyclone NP pump (< 1 m/s at the inlet of the pump), which was similar to the breathing case with the conventional NP pump. Most of the expelled particles were dispersed near the ceiling, as shown in Fig. 8(a). In this case, the coughing flow was predominant compared to any other effect including the movement of the WHT. The droplets ejected in the room may cause secondary disease transmission

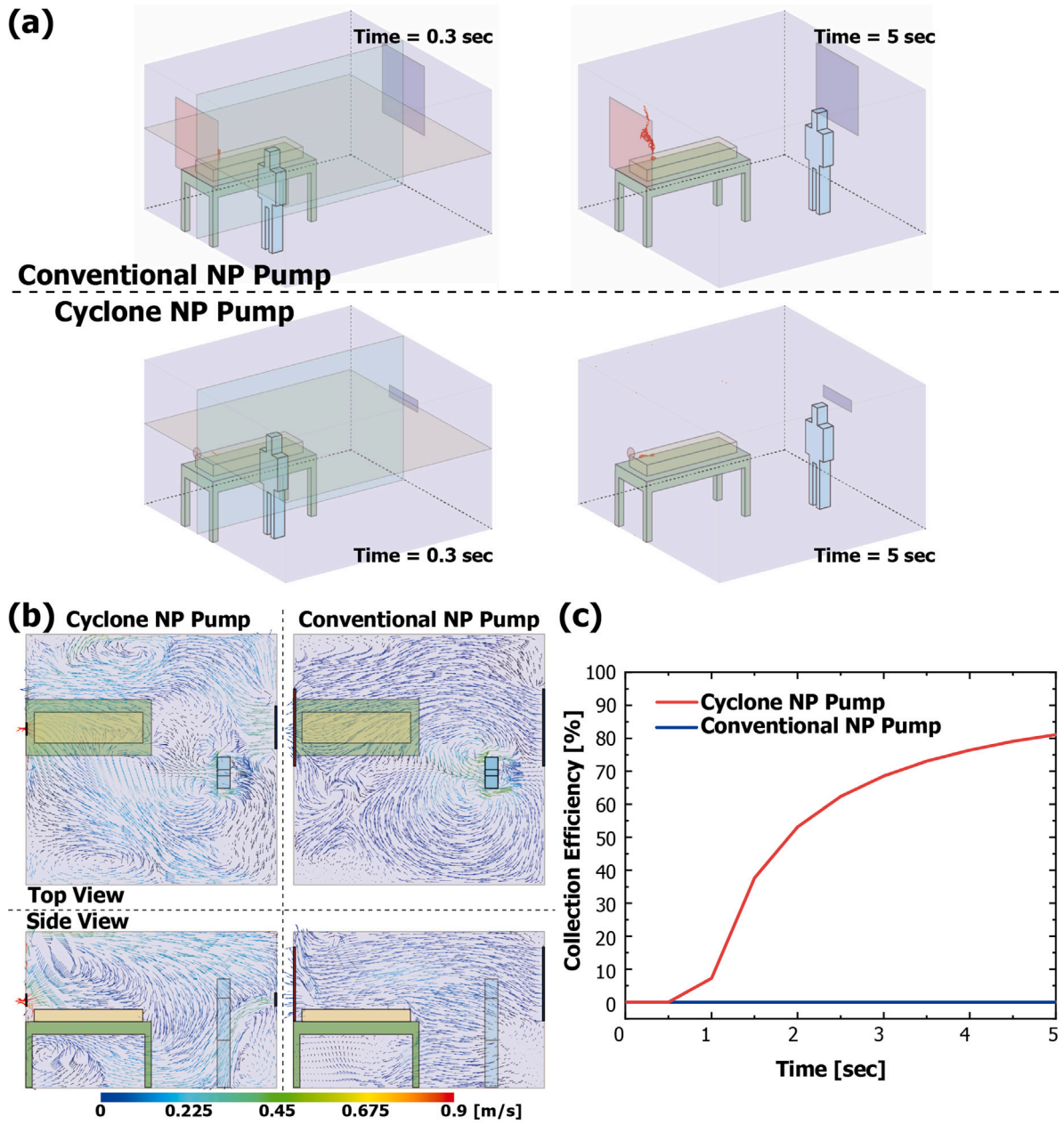

Fig. 7. Second scenario: Breathing of an infected patient on a bed. The particle-collecting performance between the conventional NP pump and the cyclone NP pump was investigated. (a) Distribution of pollutant particles at t = 0.3 and 5 s (b) Velocity vector fields in the vertical and horizontal planes. Cross-sectional planes are indicated in (a). (c) Particle collection efficiency for the cyclone NP pump and conventional NP pump for the breathing case. See Supplementary Movie 3.

in the future if there are enough contaminated pathogen particles in the room.

We found that an additional cyclone NP pump placed under the ceiling, aligned with the trajectory of coughing as illustrated in Fig. 8, could help to effectively collect the particles. In this case, to maintain the same total flow rate, we reduced the flow rate of the two cyclone NP pumps to half of the single-cyclone case. As shown in Fig. 8, the double-cyclone NP pumps were able to effectively collect the cough particles from the infected patient. While the patient kept coughing every 0.5 s, the collection efficiency was approximately 85% in 5 secs after the first cough, as demonstrated in Fig. 8(c). In this scenario, we anticipated that the double-cyclone NP pumps can rapidly purify pathogen-contaminated air from a respiratory patient, thus safeguarding medical staff.

6.4. Discussion: Effective pathogen particle removal by cyclone NP pump

Through the three different scenarios previously discussed, we confirmed the cyclone negative pressure pump, using the cyclone flow it generates, can capture contaminants adhered to the patient's body or emitted from the respiratory system. The results demonstrated the pump's superior ability to rapidly remove contaminants from random locations, significantly lowering the concentration of contaminants in the room more efficiently than conventional negative pressure pumps. Notably, unlike conventional pumps that fail to capture most contaminants transported by the turbulent flow from the patient's respiratory system, the cyclone pump exhibited remarkable performance in removing nearly all contaminants. This capability allows us to maintain a low contaminant concentration within the negative pressure room.

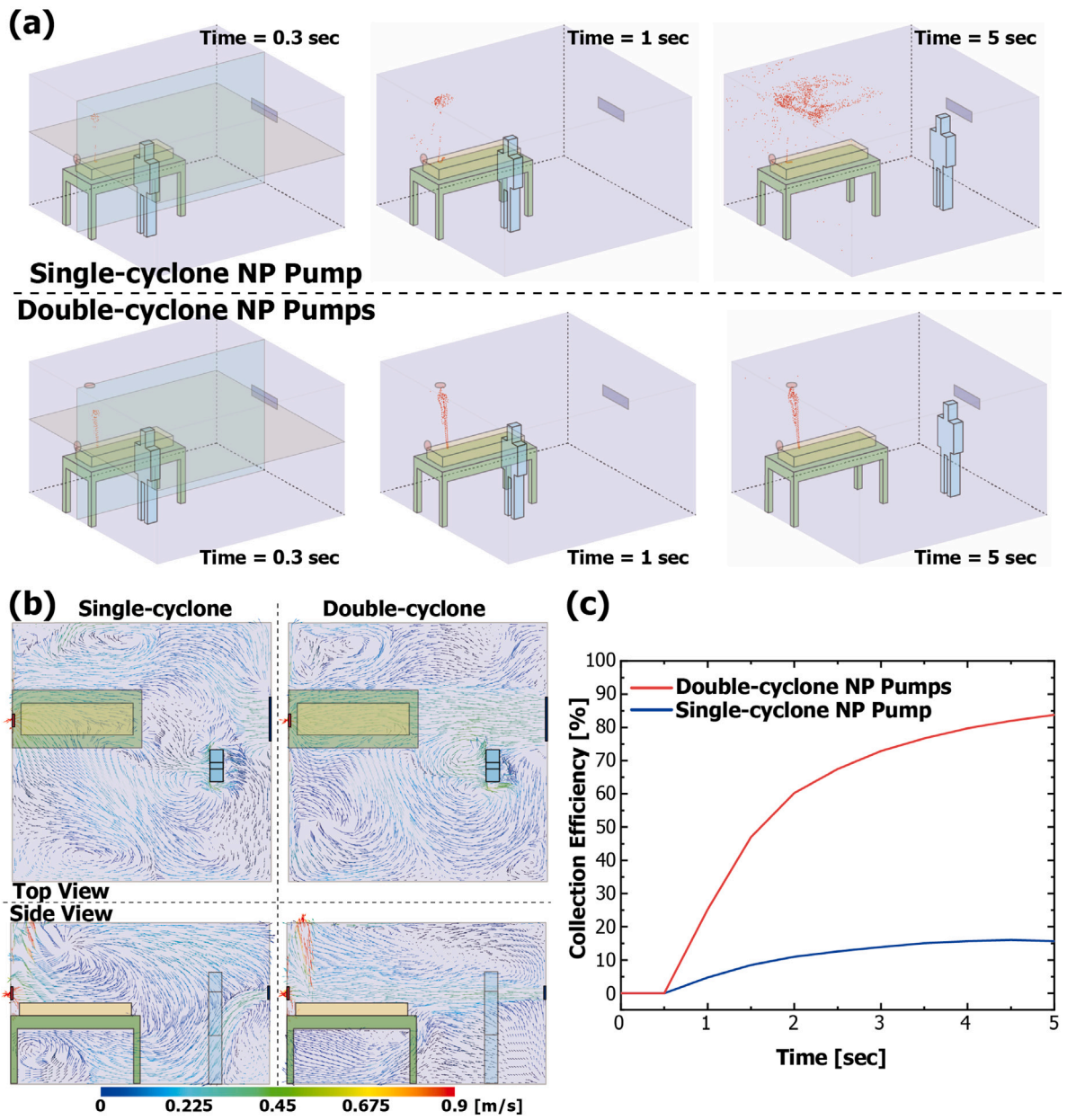

Fig. 8. Third scenario: Coughing of an infected patient on a bed. The particle-collecting performance between the single-cyclone NP pump and the double-cyclone NP pumps was compared. (a) Distribution of pollutant particles at t = 0.3, 1, and 5 s (b) Velocity vector fields in the vertical and horizontal planes. Cross-sectional planes are indicated in (a). (c) Particle collection efficiency for the single-cyclone NP pump and double-cyclone NP pumps for the coughing case. See Supplementary Movie 4.

As mentioned in Case 3, in a coughing scenario where chaotic turbulent flow occurs, a double-cyclone configuration was employed to enhance contaminant removal. Based on these results, it became evident that the installation position and orientation of the cyclone pump are crucial for efficiently capturing contaminants dispersed by high-velocity flows. In this study, we explored contaminant removal with the cyclone pump head installed on the wall. However, for future pandemic scenarios, alternative installation methods beyond wall mounting could be considered. For example, by integrating a swirler to generate cyclone flow at the ventilation inlet of the room's existing HVAC system, it is possible to create a ceiling-mounted cyclone flow configuration, as shown in Case 3. Additionally, considering the patient's posture, an arm-mounted structure, similar to shadowless operating lights used in surgical rooms, could allow the swirler's position and direction to be adjusted freely.

Therefore, the contaminant removal capability of the cyclone negative pressure pump, as demonstrated through simple scenarios in this study, could be actively applied in a variety of configurations. This would further enhance its performance in diverse situations, ensuring effective contaminant removal in future applications.

7. Conclusion

In this study, we introduced a newly developed cyclone NP pump capable of producing a directed swirling flow by interacting with the tangential flow and suction flow. We used CFD analysis to quantitatively evaluate the particle purification capabilities of the cyclone negative pressure pump. Our results demonstrated that the cyclone flow could maintain a low airborne particle concentration in a hospital room contaminated by respiratory patients. We successfully captured three different scenarios involving a completely polluted patient, a patient breathing, and a patient coughing using the cyclone NP pump. The directional swirling suction flow of the cyclone NP pump allowed it to quickly capture particles. Additionally, we proposed the use of

double-cyclone NP pumps for highly efficient particle collection with a collection efficiency of over 80% at t = 5 s for both breathing and coughing scenarios. Therefore, applying and utilizing cyclone flow can actively and effectively remove contaminants in a room while maintaining low concentrations of pollutants. In addition to hospital scenarios, as mentioned in this study, this technology can be applied to various public spaces such as city halls, libraries, and schools. It could serve as a proactive defense against the super-spreading of future respiratory infections like COVID-19 in public places frequented by large numbers of people.

CRediT authorship contribution statement

Gihyun Song: Writing – original draft, Methodology, Investigation, Formal analysis, Data curation. **Kyungcheol Jang:** Investigation, Conceptualization. **Woobin Song:** Investigation. **Wonchul Choi:** Validation, Investigation. **Simon Song:** Validation, Investigation. **Hyoungsoo Kim:** Writing – review & editing, Writing – original draft, Visualization, Validation, Supervision, Project administration, Investigation, Funding acquisition, Formal analysis, Conceptualization.

Declaration of competing interest

The authors declare that they have no known competing financial interests or personal relationships that could have appeared to influence the work reported in this paper.

Acknowledgments

This work was supported by the development of indoor airflow control and air purification technology project through National Research Council of Science and Technology (NST) funded by the Ministry of Science (CPS-21-02-KICT) in Republic of Korea and by a grant of the project for Infectious Disease Medical Safety, funded by the Ministry of Health and Welfare, Republic of Korea (RS-2022-KH131222(HG22C0099)).

Appendix A. Supplementary data

Supplementary material related to this article can be found online at https://doi.org/10.1016/j.indenv.2025.100073.

References

[1] P. Vetter, D.L. Vu, A.G. L'Huillier, M. Schibler, L. Kaiser, F. Jacquerioz, Clinical features of covid-19, Br. Med. J. 369 (2020).
[2] T. Fiolet, Y. Kherabi, C.-J. MacDonald, J. Ghosn, N. Peiffer-Smadja, Comparing COVID-19 vaccines for their characteristics, efficacy and effectiveness against SARS-CoV-2 and variants of concern: A narrative review, Clin. Microbiol. Infect. 28 (2021).
[3] A.C. Darby, J.A. Hiscox, Covid-19: variants and vaccination, Br. Med. J. 372 (2021).
[4] W.F. Wells, On air-borne infection: study II. Droplets and droplet nuclei., Am. J. Epidemiol. 20 (3) (1934) 611–618.
[5] M.W. Jennison, Atomizing of mouth and nose secretions, Aerobiology 17 (1942) 106.
[6] S. Stelzer-Braid, B.G. Oliver, A.J. Blazey, E. Argent, T.P. Newsome, W.D. Rawlinson, E.R. Tovey, Exhalation of respiratory viruses by breathing, coughing, and talking, J. Med. Virol. 81 (9) (2009) 1674–1679.
[7] J. Yan, M. Grantham, J. Pantelic, P.J.B. De Mesquita, B. Albert, F. Liu, S. Ehrman, D.K. Milton, E. Consortium, et al., Infectious virus in exhaled breath of symptomatic seasonal influenza cases from a college community, Proc. Natl. Acad. Sci. 115 (5) (2018) 1081–1086.
[8] J.L. Santarpia, D.N. Rivera, V.L. Herrera, M.J. Morwitzer, H.M. Creager, G.W. Santarpia, K.K. Crown, D.M. Brett-Major, E.R. Schnaubelt, M.J. Broadhurst, et al., Aerosol and surface contamination of SARS-CoV-2 observed in quarantine and isolation care, Sci. Rep. 10 (1) (2020) 12732.
[9] M. El Hassan, H. Assoum, N. Bukharin, H. Al Otaibi, M. Mofijur, A. Sakout, A review on the transmission of COVID-19 based on cough/sneeze/breath flows, Eur. Phys. J. Plus 137 (1) (2022) 1.
[10] P. Mick, R. Murphy, Aerosol-generating otolaryngology procedures and the need for enhanced PPE during the COVID-19 pandemic: a literature review, J. Otolaryngol. Head Neck Surg. 49 (1) (2020) 1–10.
[11] R.S. Papineni, F.S. Rosenthal, The size distribution of droplets in the exhaled breath of healthy human subjects, J. Aerosol. Med. 10 (2) (1997) 105–116.
[12] M. Abkarian, H.A. Stone, Stretching and break-up of saliva filaments during speech: A route for pathogen aerosolization and its potential mitigation, Phys. Rev. Fluids 5 (10) (2020) 102301.
[13] M. Abkarian, S. Mendez, N. Xue, F. Yang, H.A. Stone, Speech can produce jet-like transport relevant to asymptomatic spreading of virus, Proc. Natl. Acad. Sci. 117 (41) (2020) 25237–25245.
[14] L. Bourouiba, E. Dehandschoewercker, J.W. Bush, Violent expiratory events: on coughing and sneezing, J. Fluid Mech. 745 (2014) 537–563.
[15] N. Van Doremalen, T. Bushmaker, D.H. Morris, M.G. Holbrook, A. Gamble, B.N. Williamson, A. Tamin, J.L. Harcourt, N.J. Thornburg, S.I. Gerber, et al., Aerosol and surface stability of SARS-CoV-2 as compared with SARS-CoV-1, N. Engl. J. Med. 382 (16) (2020) 1564–1567.
[16] Y.-C. Tung, S.-C. Hu, T.-I. Tsai, I.-L. Chang, An experimental study on ventilation efficiency of isolation room, Build. Environ. 44 (2) (2009) 271–279.
[17] Z. Li, H. Wang, X. Zhang, T. Wu, X. Yang, Effects of space sizes on the dispersion of cough-generated droplets from a walking person, Phys. Fluids 32 (12) (2020) 121705.
[18] J.K. Lee, H.W. Jeong, Rapid expansion of temporary, reliable airborne-infection isolation rooms with negative air machines for critical COVID-19 patients, Am. J. Infect. Control 48 (7) (2020) 822–824.
[19] Z. Xu, B. Zhou, Z. Xu, B. Zhou, Importance of negative pressure wards, Dyn. Isol. Technol. Negat. Press. Isol. Wards (2017) 1–11.
[20] A. Jurelionis, L. Gagytė, T. Prasauskas, D. Čiužas, E. Krugly, L. Šeduikytė, D. Martuzevičius, The impact of the air distribution method in ventilated rooms on the aerosol particle dispersion and removal: The experimental approach, Energy Build. 86 (2015) 305–313.
[21] K. Cheong, S. Phua, Development of ventilation design strategy for effective removal of pollutant in the isolation room of a hospital, Build. Environ. 41 (9) (2006) 1161–1170.
[22] F.J. Offermann, A. Eagan, A.C. Offermann, S.S. Subhash, S.L. Miller, L.J. Radonovich, Potential airborne pathogen transmission in a hospital with and without surge control ventilation system modifications, Build. Environ. 106 (2016) 175–180.
[23] F. Memarzadeh, W. Xu, Role of air changes per hour (ACH) in possible transmission of airborne infections, Build. Simul. 5 (2012) 15–28.
[24] W. Boonmeemapasuk, N. Pochai, A risk model of airborne transmission and vaccine efficacy in an outpatient room with a ventilation system., Eng. Lett. 30 (2) (2022).
[25] S. Saran, M. Gurjar, A. Baronia, V. Sivapurapu, P.S. Ghosh, G.M. Raju, I. Maurya, Heating, ventilation and air conditioning (HVAC) in intensive care unit, Crit. Care 24 (1) (2020) 1–11.
[26] J. Cho, K. Woo, B.S. Kim, Removal of airborne contamination in airborne infectious isolation rooms, Am. Soc. Heat. Refrig. Air Cond. Eng. J. 61 (2) (2019) 8–21.
[27] N. Mingotti, R. Wood, C. Noakes, A.W. Woods, The mixing of airborne contaminants by the repeated passage of people along a corridor, J. Fluid Mech. 903 (2020).
[28] M. Yanai, Formation of tropical cyclones, Rev. Geophys. 2 (2) (1964) 367–414.
[29] H. Kim, K. Jang, S. Song, W. Choi, W. Song, A Negative Pressure Mobile Device Using Cyclone, (no. 102339302) South Korea, 2021.
[30] S.K. Ahmed, R.M. Ali, M.M. Lashin, F.F. Sherif, Designing a new fast solution to control isolation rooms in hospitals depending on artificial intelligence decision, Biomed. Signal Process. Control 79 (2023) 104100.
[31] J. Wang, T.-T. Chow, Numerical investigation of influence of human walking on dispersion and deposition of expiratory droplets in airborne infection isolation room, Build. Environ. 46 (10) (2011) 1993–2002.
[32] B.A. Edge, E.G. Paterson, G.S. Settles, Computational study of the wake and contaminant transport of a walking human, J. Fluids Eng. 127 (5) (2005) 967–977.
[33] G.J. Bastien, P.A. Willems, B. Schepens, N.C. Heglund, Effect of load and speed on the energetic cost of human walking, Eur. J. Appl. Physiol. 94 (1) (2005) 76–83.
[34] Y. Wu, N. Gao, The dynamics of the body motion induced wake flow and its effects on the contaminant dispersion, Build. Environ. 82 (2014) 63–74.
[35] T.-T. Chow, J. Wang, Dynamic simulation on impact of surgeon bending movement on bacteria-carrying particles distribution in operating theatre, Build. Environ. 57 (2012) 68–80.
[36] Y.-C. Shih, C.-C. Chiu, O. Wang, Dynamic airflow simulation within an isolation room, Build. Environ. 42 (9) (2007) 3194–3209.
[37] Ansys, Fluent 12.0 Theory Guide, Ansys Inc., USA, 2011.
[38] A. Khosronejad, S. Kang, F. Wermelinger, P. Koumoutsakos, F. Sotiropoulos, A computational study of expiratory particle transport and vortex dynamics during breathing with and without face masks, Phys. Fluids 33 (6) (2021) 066605.
[39] W.C. Hinds, Y. Zhu, Aerosol Technology: Properties, Behavior, and Measurement of Airborne Particles, John Wiley & Sons, 2022.

[40] N. Zahari, M. Zawawi, L. Sidek, D. Mohamad, Z. Itam, M. Ramli, A. Syamsir, A. Abas, M. Rashid, Introduction of discrete phase model (DPM) in fluid flow: a review, AIP Conf. Proc. 2030 (1) (2018) 020234.
[41] B. Zhao, Y. Zhang, X. Li, X. Yang, D. Huang, Comparison of indoor aerosol particle concentration and deposition in different ventilated rooms by numerical method, Build. Environ. 39 (1) (2004) 1–8.
[42] E. Stamhuis, W. Thielicke, PIVlab–towards user-friendly, affordable and accurate digital particle image velocimetry in MATLAB, J. Open Res. Softw. 2 (1) (2014) 30.
[43] R.J. Adrian, J. Westerweel, Particle Image Velocimetry, (no. 30) Cambridge University Press, 2011.
[44] Infection prevention and control during transfer and transport of patients with suspected or confirmed COVID-19, World Heal. Organ. Reg. Off. West. Pac. (2021).
[45] L.-Q. Li, T. Huang, Y.-Q. Wang, Z.-P. Wang, Y. Liang, T.-B. Huang, H.-Y. Zhang, W. Sun, Y. Wang, COVID-19 patients' clinical characteristics, discharge rate, and fatality rate of meta-analysis, J. Med. Virol. 92 (6) (2020) 577–583.
[46] Q. Yang, T.K. Saldi, P.K. Gonzales, E. Lasda, C.J. Decker, K.L. Tat, M.R. Fink, C.R. Hager, J.C. Davis, C.D. Ozeroff, et al., Just 2% of SARS-CoV-2- positive individuals carry 90% of the virus circulating in communities, Proc. Natl. Acad. Sci. 118 (21) (2021) e2104547118.
[47] M. Marks, P. Millat-Martinez, D. Ouchi, C. h Roberts, A. Alemany, M. Corbacho-Monné, M. Ubals, A. Tobias, C. Tebé, E. Ballana, et al., Transmission of COVID-19 in 282 clusters in Catalonia, Spain: a cohort study, Lancet Infect. Dis. 21 (5) (2021) 629–636.
[48] S. Karimzadeh, R. Bhopal, H.N. Tien, Review of infective dose, routes of transmission and outcome of COVID-19 caused by the SARS-COV-2: comparison with other respiratory viruses, Epidemiol. Infect. 149 (2021) e96.
[49] X. He, E.H. Lau, P. Wu, X. Deng, J. Wang, X. Hao, Y.C. Lau, J.Y. Wong, Y. Guan, X. Tan, et al., Temporal dynamics in viral shedding and transmissibility of COVID-19, Nature Med. 26 (5) (2020) 672–675.
[50] L.M. Brosseau, K. Escandón, A.K. Ulrich, A.L. Rasmussen, C.J. Roy, G.J. Bix, S.V. Popescu, K.A. Moore, M.T. Osterholm, Severe acute respiratory syndrome coronavirus 2 (SARS-CoV-2) dose, infection, and disease outcomes for coronavirus disease 2019 (COVID-19): a review, Clin. Infect. Dis. 75 (1) (2022) e1195–e1201.
[51] B. Scharfman, A. Techet, J. Bush, L. Bourouiba, Visualization of sneeze ejecta: steps of fluid fragmentation leading to respiratory droplets, Exp. Fluids 57 (2016) 1–9.
[52] B.T. Gidreta, H. Kim, Effects of physical property changes of expelled respiratory liquid on atomization morphology, J. Fluid Mech. 960 (2023) A10.
[53] H. Li, F.Y. Leong, G. Xu, Z. Ge, C.W. Kang, K.H. Lim, Dispersion of evaporating cough droplets in tropical outdoor environment, Phys. Fluids 32 (11) (2020) 113301.
[54] S.-B. Kwon, J. Park, J. Jang, Y. Cho, D.-S. Park, C. Kim, G.-N. Bae, A. Jang, Study on the initial velocity distribution of exhaled air from coughing and speaking, Chemosphere 87 (11) (2012) 1260–1264.
[55] S. Asadi, A.S. Wexler, C.D. Cappa, S. Barreda, N.M. Bouvier, W.D. Ristenpart, Aerosol emission and superemission during human speech increase with voice loudness, Sci. Rep. 9 (1) (2019) 1–10.